

Automatic procedure for aberrations compensation in digital holographic microscopy

Tristan Colomb^a, Jonas Kühn^a, Etienne Cuche^b, Florian Charrière^a, Frédéric Montfort^b, Anca Marian^a, Nicolas Aspert^b, Pierre Marquet^c and Christian Depeursinge^a

^aEcole Polytechnique Fédérale de Lausanne (EPFL), Imaging and Applied Optics Institute,
CH-1015 Lausanne, Switzerland;

^bLyncée Tec SA, PSE-A, CH-1015 Lausanne, Switzerland;

^cCentre de Neurosciences Psychiatriques, Département de psychiatrie DP-CHUV, Site de Cery,
1008 Prilly-Lausanne, Switzerland

ABSTRACT

Digital Holographic Microscopy (DHM) is a powerful imaging technique allowing, from a single amplitude image acquisition (hologram), the reconstruction of the entire complex wave front (amplitude and phase), reflected by or transmitted through an object. Because holography is an interferometric technique, the reconstructed phase leads to a sub-wavelength axial accuracy (below $\lambda/100$). Nevertheless, this accuracy is difficult to obtain from a single hologram. Indeed, the reconstruction process consisting to process the hologram with a digital reference wave (similar to classical holographic reconstruction) seems to need a-priori knowledge about the physical values of the setup. Furthermore, the introduction of a microscope objective (MO), used to improve the lateral resolution, introduces a wave front curvature in the object wave front. Finally, the optics of the set-up can introduce different aberrations that decrease the quality and the accuracy of the phase images. We propose here an automatic procedure allowing the adjustment of the physical values and the compensation for the phase aberrations. The method is based on the extraction of reconstructed phase values, along line profiles, located on or around the sample, in assumed to be flat area, and which serve as reference surfaces. The phase reconstruction parameters are then automatically adjusted by applying curve-fitting procedures on the extracted phase profiles. An example of a mirror and a USAF test target recorded with high order aberrations (introduced by a thick tilted plate placed in the set-up) shows that our procedure reduces the phase standard deviation from 45 degrees to 5 degrees.

Keywords: Digital holography, Aberration compensation, Microscopy, Phase measurement

1. INTRODUCTION

DHM is a powerful instrument to study microscopic specimens by retrieving the amplitude and phase of the wave reflected by the specimen or transmitted through it. Phase reconstruction is of particular interest since it enables surface topography measurements with nanometer vertical resolution.¹ Several methods are proposed for phase measurements in digital holography. In line techniques² use phase shifting procedures that require several hologram acquisitions, at least three, and additional means, such as a piezoelectric transducer, for controlling the phase of the reference wave. In off-axis configurations, Schnars *et al.*³ have demonstrated the possibility to measure specimen deformations by evaluating the phase difference between two states of the specimen. However, this double exposure technique does not give the absolute phase introduced by the specimen.

A solution for absolute phase measurements is proposed by Cuche *et al.* in 1999. They introduce the concept of digital reference wave,¹ that compensates the role of the reference wave in an off-axis geometry, and the concept of digital phase mask,⁴ which is introduced to compensate for the wavefront deformation associated to the use of a microscope objective (MO). These two quantities are defined numerically as arrays of complex numbers, computed using a set of parameters, called phase reconstruction parameters, whose values must be precisely defined so that these computed data fit as close as possible their experimental equivalences. This

Further author information: E-mail: tristan.colomb@a3.epfl.ch

approach enables absolute phase reconstruction, with a single hologram acquisition. However, as proposed initially, the procedure for the phase reconstruction parameters adjustment was not automated and required a prior knowledge of the parameters values, making the method not user friendly.

In the other hand, different kinds of aberration are successfully removed as spherical aberration,⁵ chromatic aberration,⁶ astigmatism,^{7,8} anamorphism,^{9,10} or longitudinal image shifting introduced by a beam splitter cube.¹¹

In this paper, we introduce a new digital phase mask that can be seen as a Numerical Parametric Lens (NPL) that compensates for the role of the reference digital wave, the curvature induced by the MO and a complete aberration compensation. Furthermore, we show that a simple and automatic procedure computes this NPL without prior knowledge of physical values.

2. EXPERIMENTAL CONFIGURATION

Two main configurations exist for the implementation of DHM: a first one [Fig. 1(a)] for transmission imaging and a second one [Fig. 1(b)] for reflection imaging. In both cases the basic architecture is that of a modified Mach-Zehnder interferometer. The combination of a neutral density filter, a half-wave plate and a polarizing beam splitter are used for the adjustment of the intensities in the reference and object arms.

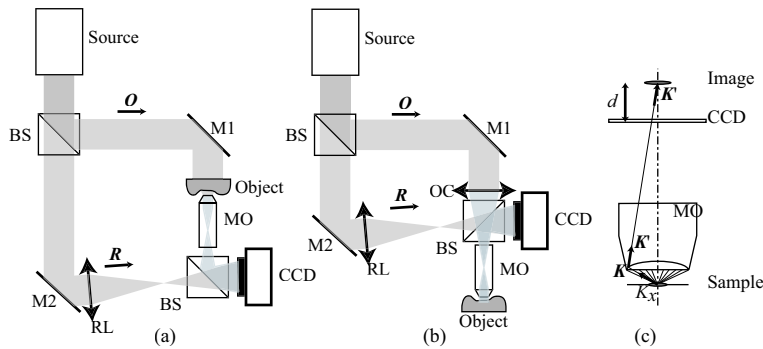


Figure 1. Microscope configuration for (a) transmission and (b) reflection. PBS, polarizing beam splitter; BS, beam splitter, $\lambda/2$, half-wave plate; M1, M2 mirrors; C, lens used as condenser that focalized in the back focal lens of the microscope objective (MO); RL, reference lens; NF, neutral filter.(c)Use of a lens or microscope objective to match the sampling capacity of a CCD placed in the plane of the hologram with the spatial spectrum of the object.

In both microscope configurations, a MO collects the object wave \mathbf{O} transmitted or reflected by the specimen, and produces a magnified image of the specimen behind the CCD camera at a distance d [Fig. 1(c)]. As explained in details in Ref. 12, this situation can be considered to be equivalent to a holographic configuration without MO with an object wave \mathbf{O} emerging directly from the magnified image of the specimen and not from the specimen itself. Very high resolution can be obtained by MO with a high numerical aperture (NA). Indeed, the role of this high NA MO is to provide a simple mean to adapt the sampling capacity of the camera to the information content of the hologram.¹³ As illustrated in Fig. 1(c), a lens or a MO achieve a reduction of the K_x, K_y components of the \mathbf{K} vector components in the specimen plane perpendicular to the optical axis. The reduction factor is given by the magnification of the MO. The new components K'_x, K'_y of the \mathbf{K}' wavevector of the beam after having crossed the MO can be made as small as required by the Shannon theorem applied to the sampling capacity dictated by the pixel size of the camera. Using a high magnification objective, the match can be optimized. At the same time, by maximizing the NA, the transverse resolution can be pushed to the limit of diffraction and sub-micron resolution can be easily achieved (ordinarily better than 600nm).

At the exit of the interferometer the interference between the object wave \mathbf{O} and the reference wave \mathbf{R} creates the hologram intensity:

$$I_H(x, y) = (\mathbf{R} + \mathbf{O})(\mathbf{R} + \mathbf{O})^* = |\mathbf{R}|^2 + |\mathbf{O}|^2 + \mathbf{R}^* \mathbf{O} + \mathbf{R} \mathbf{O}^*. \quad (1)$$

A lens could be introduced in the reference arm (RL) to produce a spherical reference wave with a curvature in the CCD plane very similar to the curvature induced by the MO. This permits to have a hologram composed with equal spaced straight fringes. This hologram is digitalized and recorded by a black and white CCD camera and then transmitted to a computer. The digital hologram $I_H(k, l)$ is an array of $N \times N$ (usually 512×512 or 1024×1024) 8-bit-encoded numbers resulting from the two dimensional sampling of $I_H(x, y)$ by the CCD camera:

$$I_H(k, l) = \int_{k\Delta x - \Delta x/2}^{k\Delta x + \Delta x/2} \int_{l\Delta y - \Delta y/2}^{l\Delta y + \Delta y/2} I_H(x, y) dx dy. \quad (2)$$

where k, l are integers and $\Delta x, \Delta y$ define the sampling intervals in the hologram plane (pixel size). A hologram of a pollen grain recorded with a transmission setup is presented in Fig. 2.

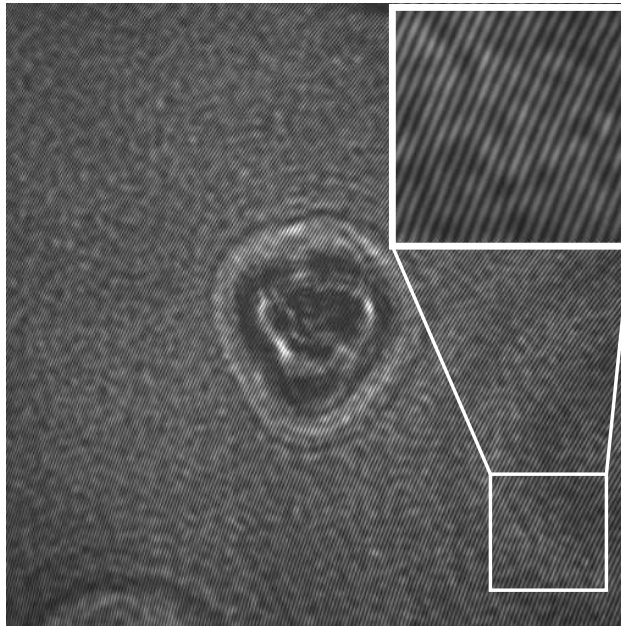


Figure 2. Digital hologram of a pollen grain recorded with a X40 MO in a transmission setup.

3. RECONSTRUCTION ALGORITHM

In Ref. 4, the algorithm for hologram reconstruction in the Fresnel approximation, was formulated as follows:

$$\Psi(\xi, \eta) = \Phi(\xi, \eta) \cdot \frac{\exp(i2\pi d/\lambda)}{i\lambda d} \exp\left[\frac{i\pi}{\lambda d}(\xi^2 + \eta^2)\right] \cdot \iint \mathbf{R}_D(x, y) I_H(x, y) \exp\left[\frac{i\pi}{\lambda d}((x - \xi)^2 + (y - \eta)^2)\right] dx dy. \quad (3)$$

This expression describes the Fresnel propagation of the reconstructed wavefront Ψ over a distance d , from the hologram plane oxy to the observation plane (or reconstruction plane) $o\xi\eta$. The digital reference wave \mathbf{R}_D introduced in Ref. 1, and the digital phase mask Φ introduced in Ref. 4 play a major role in the phase reconstruction. \mathbf{R}_D is defined as a computed replica of the experimental reference wave \mathbf{R} . Assuming an hologram recorded in the off-axis geometry with a plane reference wave, \mathbf{R}_D is written:

$$\mathbf{R}_D(x, y) = \exp\left[i\frac{2\pi}{\lambda}(k_x x + k_y y) + i\varphi(t)\right], \quad (4)$$

where the parameters k_x, k_y define the propagation direction, and $\varphi(t)$ the phase delay between the object and reference waves, which varies during time due to external perturbations, such as mechanical vibrations. As explained in Ref. 1, for proper phase reconstruction, the k_x and k_y values must be adjusted, so that the

propagation direction of the computed wave-front \mathbf{R}_D fits the propagation direction of the experimental wave \mathbf{R} . As explained in Ref. 4, the role of Φ is to compensate for the wave-front curvature that appears when a MO is used to improve the transverse resolution. The phase curvature can be corrected by multiplication of the reconstructed wave front with a simple quadratic model⁴:

$$\Phi(\xi, \eta) = \exp \left[\frac{-i\pi}{\lambda C} (\xi^2 + \eta^2) \right], \quad (5)$$

where C is the parameter that has to be adjusted to compensate for this curvature. The reconstruction procedure of Eq. 3 involves four parameters: k_x , k_y and C , for phase reconstruction, and the reconstruction distance d for image focusing. This formulation suffers from several drawbacks:

- i) As the digital reference wave is located inside the Fresnel integral, changing the k_x and k_y shifts the reconstructed images in the observation plane.
- ii) The model used to compute the digital phase mask is limited to the second order, and fails therefore in compensating for higher order aberrations (e.g. astigmatism and spherical).
- iii) Adjusting manually the k_x , k_y and C parameters is a complex task that requires expertise and a prior knowledge of their values.

We will describe how the reconstruction procedure can be improved in order to suppress these drawbacks. It can be demonstrated that the digital reference wave \mathbf{R}_D in Eq. 3 can be replaced by a pseudo-reference wave \mathbf{R}' outside the integral by using the modulation property of the Fresnel transform¹⁴:

$$\Psi(\xi, \eta) = \Phi(\xi, \eta) \cdot \mathbf{R}'(\xi, \eta) \cdot \frac{\exp(i2\pi d/\lambda)}{i\lambda d} \exp \left[\frac{i\pi}{\lambda d} (\xi^2 + \eta^2) \right] \cdot \int \int I_H(x, y) \exp \left[\frac{i\pi}{\lambda d} ((x - \xi)^2 + (y - \eta)^2) \right] dx dy. \quad (6)$$

where \mathbf{R}' is the pseudo-reference wave

$$\mathbf{R}'(\xi, \eta) = \exp \left[i \frac{2\pi}{\lambda} (k_x \xi + k_y \eta) + i\varphi'(k_x, k_y, t) \right]. \quad (7)$$

This means that passing the digital reference wave outside the Fresnel integral is a straightforward operation that conserves the plane wave nature of the wavefront. In other words, for phase reconstruction with DHM, it means that the effects of the off-axis geometry has the appearance of a tilt aberration in the observation plane. This tilt can be compensated by multiplying the reconstructed wavefront with a correcting term calculated with the mathematical model of a plane wave. Compared to the former method [Eq. 3], the great advantage is that the adjustment of this pseudo-reference wave does not shift the image in the reconstruction plane and the propagation integral does not need to be recomputed if the parameters k_x and k_y change.

4. NUMERICAL PARAMETRIC LENS

Equation 6 describes the reconstruction algorithm as the Fresnel transform of the hologram intensity I_H multiplied by the product of the digital phase mask Φ with the pseudo digital reference wave \mathbf{R}' . As $\Phi(\xi, \eta)$ and $\mathbf{R}'(\xi, \eta)$ appear now outside the Fresnel integral, they can be merged in a single entity, and the reconstruction algorithm becomes:

$$\begin{aligned} \Psi(\xi, \eta) &= \Gamma^I(\xi, \eta) \cdot \frac{\exp(i2\pi d/\lambda)}{i\lambda d} \exp \left[\frac{i\pi}{\lambda d} (\xi^2 + \eta^2) \right] \cdot \int \int I_H(x, y) \exp \left[\frac{i\pi}{\lambda d} ((x - \xi)^2 + (y - \eta)^2) \right] dx dy \\ &= \Gamma^I(\xi, \eta) \cdot \Omega(\xi, \eta), \end{aligned} \quad (8)$$

where according to Eqs. 5 and 7 we have:

$$\Gamma^I(\xi, \eta) = \exp \left[\frac{i\pi}{\lambda} \left(2k_x \xi + 2k_y \eta - \frac{\xi^2 + \eta^2}{C} \right) + i\varphi'(k_x, k_y, t) \right]. \quad (9)$$

This new formulation of the digital phase mask involves four reconstruction parameters; k_x and k_y for compensating for the tilt aberration due to the off-axis geometry, the phase offset φ' for compensating for the phase delay between the object and reference waves, and C for compensating for a quadratic wave-front curvature. This expression for the digital phase mask can be seen as a Numerical Parametric Lens (NPL) placed in the Image plane and can be written in a second order polynomial:

$$\Gamma^I(\xi, \eta) = \exp \left[-i \frac{2\pi}{\lambda} (P_{00} + P_{10}\xi + P_{01}\eta + P_{20}\xi^2 + P_{02}\eta^2) \right]. \quad (10)$$

where P_{hv} define a new set of phase reconstruction parameters. The physical constants (λ , C and π) are suppressed from the definition of the P_{hv} parameters. But the corresponding physical quantities can be evaluated if necessary. For example:

$$P_{00} = -\frac{\lambda}{2\pi} \varphi', \quad (11)$$

$$P_{10} = -k_x, \quad P_{01} = -k_y, \quad (12)$$

$$P_{20} = P_{02} = \frac{1}{2C}. \quad (13)$$

The expression of the NPL defined in Eq. 10 covers a very limited range of situations. In order to enable the compensation for higher orders aberrations, we generalize this formulation by increasing the polynomial order of the NPL:

$$\Gamma^I(\xi, \eta) = \exp \left[-i \frac{2\pi}{\lambda} \sum_{\alpha=0}^H \sum_{\beta=0}^V P_{\alpha\beta} \cdot \xi^\alpha \eta^\beta \right], \quad (14)$$

where $P_{\alpha\beta}$ define a set of reconstruction parameters, H and V define the polynomial orders in the horizontal and vertical directions respectively. The discrete formulation of Eq. 14 is

$$\Gamma^I(m, n) = \exp \left[-i \frac{2\pi}{\lambda} \sum_{\alpha=0}^H \sum_{\beta=0}^V P_{\alpha\beta} \cdot m^\alpha n^\beta \right]. \quad (15)$$

5. AUTOMATIC NUMERICAL PARAMETRIC LENS ADJUSTMENT

5.1. Principle

We will now describe the iterative procedure that allows the adjustment of the first four parameters (P_{00} , P_{10} , P_{01} , P_{20} , P_{02}) defined in Eq. 14. To illustrate the procedure, a hologram of a pollen grain taken in a transmission setup [Fig. 1(b)] with a X40 MO is used. The hologram is presented in Fig. 2. We can see the curvature of the fringes pattern due to the presence of the MO.

After hologram apodization¹⁵ and a spatial frequency filtering,¹² the reconstructed wavefront $\Omega(\xi, \eta)$ (Eqs. 8) is computed in Single Fourier Transform Formulation (the Convolution formulation can also be used without losing generality) and the Region Of Interest (ROI), corresponding to the location of the real image, is delineated inside the image plane.

Figure 3(a) presents the ROI of the phase image of the wavefront Ω . As no NPL is applied and as the phase is defined as modulo 2π , the phase seems to be randomly distributed. In fact, this phase reconstruction contains the information that will be used to adjust automatically the phase reconstruction parameters. Indeed the reconstructed phase of Fig. 3(a), is the addition of three contributions:

- i) The absolute phase of the specimen

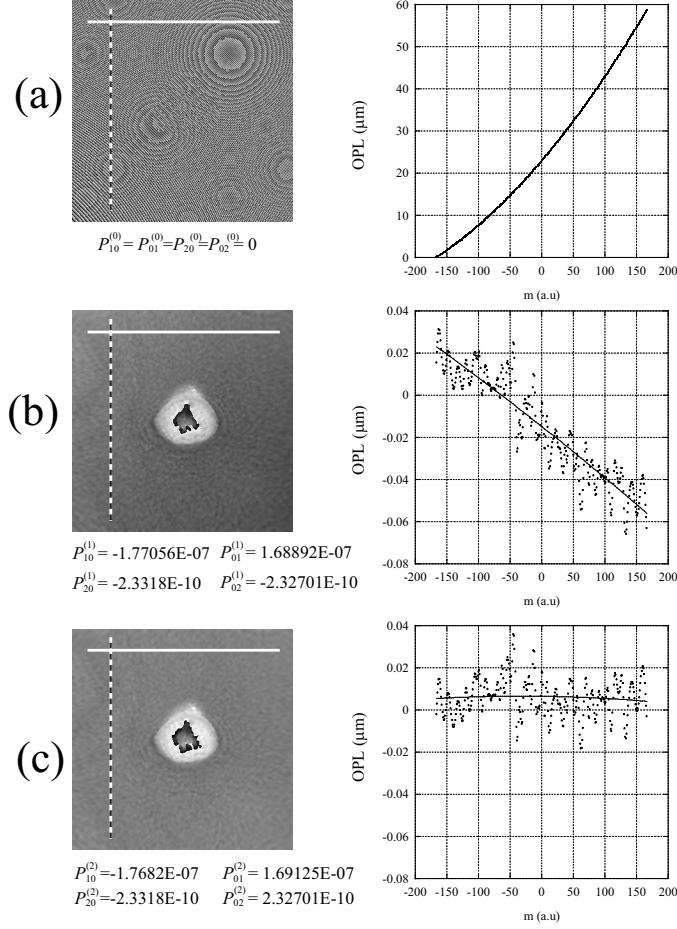


Figure 3. Automatic adjustment of a second order NPL. The left column presents phase images obtained for different obtained values of the parameters computed from the white horizontal and vertical profiles. The right column presents plots of unwrapped optical path length, and fitted curve, for the horizontal direction. (a) Initial phase reconstruction parameters, (b) after first iteration, (c) second iteration.

- ii) The tilt aberration due to the off-axis geometry
- iii) The aberrations, or wavefront deformations induced by the setup, in particular the curvature produced by the MO.

The method for the adjustment of the phase reconstruction parameters consists in evaluating the last two contributions, in areas where the specimen contribution is known to be constant, or in other words in a flat reference area located near, or on the specimen. First, no phase aberration is assumed, excepting tilt due to the off-axis geometry and quadratic phase curvature induced by the MO. The first operation consists in defining two perpendicular lines [see Fig. 3(a)], one for each direction m and n , respectively the horizontal and the vertical directions (the origin is defined in the center of the ROI). Along both lines, phase profiles are extracted. With strongly aberrated wave fronts such as those presented in Fig. 3(a), the phase variation along the selected profiles exceed several times 2π . that produces phase jumps (between $-\pi$ and $+\pi$). These phase jumps are suppressed by the application of a standard 1D phase unwrapping algorithm. The resulting continuous phase profiles are then converted to optical path length [multiplication of the phase value by $\lambda/(2\pi)$] to be fitted with a 1D polynomial function. This conversion is done to compute the parameters independently from the wavelength. Let us assume a correction limited to the second order, and let us define

$$Y_h = a_0 + a_1x + a_2x^2 \quad (16)$$

$$Y_v = b_0 + b_1 y + b_2 y^2. \quad (17)$$

the two optical path length curves fitted along respectively the horizontal, and the vertical profiles. In this case NPL becomes simply:

$$\Gamma^I(m, n) = \exp \left[-i \frac{2\pi}{\lambda} (a_1 m + b_1 n + a_2^2 m^2 + b_2^2 n^2) \right]. \quad (18)$$

where $a_1 = P_{10}$ and $b_1 = P_{01}$ compensate for the tilt aberration along respectively the horizontal and vertical directions, and where $a_2 = P_{20}$, and $b_2 = P_{02}$ compensate for a second order wavefront curvature along respectively the horizontal and vertical directions. In principle, this procedure should work immediately, but as shown in Fig. 3(b), residual aberrations may persist. The reason for this is that, without correction [Fig. 3(a)], or with initial parameters too far from the correct values, the phase distribution varies so rapidly that several phase jumps may occur over distances smaller than one pixel. In this case, the phase unwrapping procedure cannot work properly. To avoid this effect, the procedure described above is applied iteratively, starting from initial values $P_{\alpha\beta}^{(0)}$ provided by a first evaluation. At each iteration, the coefficients of the fitted curve are added to the parameters from the previous iteration. Let us define the fitting curves of the two profiles defined on the reconstructed phase image at iteration j :

$$\begin{aligned} Y_h^{(j)} &= a_0^{(j)} + a_1^{(j)} x + a_2^{(j)} x^2 \\ Y_v^{(j)} &= b_0^{(j)} + b_1^{(j)} y + b_2^{(j)} y^2. \end{aligned} \quad (19)$$

The new phase reconstruction parameters become ($k = 1, 2$):

$$\begin{aligned} P_{k0}^{(j)} &= P_{k0}^{(j-1)} + a_k^{(j)} \\ P_{0k}^{(j)} &= P_{0k}^{(j-1)} + b_k^{(j)}. \end{aligned} \quad (20)$$

The procedure converges very rapidly to the optimal values, and less than four iterations are sufficient in most cases [see Fig. 3(c)].

A first approach for higher order corrections consists simply in increasing the polynomial order of the fit along the horizontal and vertical directions and in applying the same procedure to compute the phase reconstruction parameters. In the case of one profile procedure, Eq. 17 becomes

$$Y_h = a_0 + a_1 x + a_2 x^2 + \dots + a_\alpha x^\alpha + \dots + a_H x^H \quad (21)$$

$$Y_v = b_0 + b_1 y + b_2 y^2 + \dots + b_\beta y^\beta + \dots + b_V y^V. \quad (22)$$

where H and V are respectively the polynomial order for the horizontal and vertical directions. The computed parameters are therefore $P_{\alpha 0} = a_\alpha$ and $P_{0\beta} = b_\beta$ ($\alpha \leq H$, $\beta \leq V$).

However, according to the general formulation of the NPL [Eq. 15], this procedure is effective only for the calculation of $P_{\alpha 0}$ and $P_{0\beta}$ terms. For the $P_{\alpha\beta}$ cross-terms correction, it is necessary to extract others profiles in the image. The definition of these profiles and the solution of the corresponding equations systems allow to compute higher order crossed-terms. The details of the calculus are given in the next sections.

5.2. P_{11} computation

Let us consider first the second order crossed term parameter P_{11} , which can be evaluated by defining two profiles of slopes ± 1 , along the diagonals of the image: $n = m + \tau$ ($y = x + cst$) and $n = -m + \nu$ ($y = x - cst$). The second order phase component of the NPL along the first profile is

$$\begin{aligned} \varphi_{+1} &= P_{10}m + P_{01}(m + \tau) + P_{20}m^2 + P_{02}(m + \tau)^2 + P_{11}m(m + \tau) \\ &= (P_{20} + P_{02} + P_{11})m^2 + (P_{10} + P_{01} + 2P_{02}\tau + P_{11}P_{02})m + (P_{01}\tau + P_{02}\tau^2) \\ &= a_2^{(+1)}m^2 + a_1^{(+1)}m + a_0^{(+1)}. \end{aligned} \quad (23)$$

Similarly, along the other profile, we have

$$\varphi_{-1} = (P_{20} + P_{02} - P_{11}) m^2 + \dots = a_2^{(-1)} m^2 + a_1^{(-1)} m + a_0^{(-1)}, \quad (24)$$

which yields

$$P_{11} = \frac{a_2^{(+1)} - a_2^{(-1)}}{2}, \quad (25)$$

where $a_2^{(+1)}$ and $a_2^{(-1)}$ are the second order coefficient of the polynomial fit along the diagonal profiles, respectively $y = x + cst$ and $y = -x + cst$. Henceforth we will note $a_i^{(+j)}$ the i^{th} order coefficient of the polynomial fit along a profile of slope j : $y = jx + cst$.

5.3. P_{12} and P_{21} computation

In order to compute the third order crossed terms P_{12} and P_{21} , we need to consider two additional profiles at $n = 2m + \tau$ ($y = 2x + cst$) and $n = -2m + \nu$ ($y = -2x + cst$). Along the two profiles of slope ± 1 , the relations to the third order hold

$$\begin{aligned} \varphi_{+1} &= (P_{30} + P_{03} + P_{12} + P_{21}) m^3 + \dots = a_3^{(+1)} m^3 + \dots \\ \varphi_{-1} &= (P_{30} - P_{03} + P_{12} - P_{21}) m^3 + \dots = a_3^{(-1)} m^3 + \dots \end{aligned} \quad (26)$$

For the profiles of slope ± 2 , we have

$$\begin{aligned} \varphi_{+2} &= (P_{30} + 8P_{03} + 4P_{12} + 2P_{21}) m^3 + \dots = a_3^{(+2)} m^3 + \dots, \\ \varphi_{-2} &= (P_{30} - 8P_{03} + 4P_{12} - 2P_{21}) m^3 + \dots = a_3^{(-2)} m^3 + \dots \end{aligned} \quad (27)$$

Eliminating the terms P_{30} and P_{03} in these equations yield

$$P_{12} = \frac{a_3^{(+2)} + a_3^{(-2)} - a_3^{(+1)} - a_3^{(-1)}}{6}, \quad (28)$$

$$P_{21} = \frac{2}{3} \left(a_3^{(+1)} - a_3^{(-1)} - \frac{a_3^{(+2)} - a_3^{(-2)}}{8} \right). \quad (29)$$

By analogy, the definition of others profiles and the solving of resulting equations systems allows to compute higher order crossed-terms.

6. EXPERIMENTAL VALIDATION

To illustrate the procedure for higher orders and crossed terms corrections, an experimental aberrated phase distribution is studied by introducing a tilted thick plate between the beam splitter and the CCD camera in the reflection setup [Fig. 1(a)]. A hologram of a mirror is recorded with a X10 MO. The Fig. 4(a) presents the phase reconstruction of this hologram without aberration compensation.

Figure 4 presents the computed phase reconstructions for increasing orders of correction from (a) to (e). The offset parameter P_{00} is adjusted to have a mean phase value on the entire image equal to zero. The efficiency of the correction is evaluated by measuring the Standard Deviation (std) of the phase distribution over the entire field of view. As can be seen, std decreases rapidly to 5.1 degrees. In this case, the procedure computes the following coefficients values: $P_{10} = 3.1382 \cdot 10^{-7}$, $P_{01} = -3.1735 \cdot 10^{-7}$, $P_{20} = -1.0635 \cdot 10^{-9}$, $P_{02} = -1.0726 \cdot 10^{-9}$, $P_{30} = -3.4615 \cdot 10^{-14}$, $P_{03} = 3.3820 \cdot 10^{-14}$, $P_{40} = -1.0333 \cdot 10^{-16}$, $P_{04} = 1.1985 \cdot 10^{-16}$, $P_{11} = -1.3596 \cdot 10^{-11}$, $P_{12} = -4.6197 \cdot 10^{-14}$, $P_{21} = 3.4313 \cdot 10^{-14}$. The residual noise may have several origins, such as uncorrected aberrations, surface defects on the mirror or on optical components of the microscope, as well as spatial phase fluctuations caused by dusts, parasitic reflections or diffraction effects.

A mirror is an ideal specimen because long profiles can be taken to evaluate the phase reconstruction parameters. As presented in Fig. 5, coefficients evaluated using a mirror can be used as calibrated values to correct

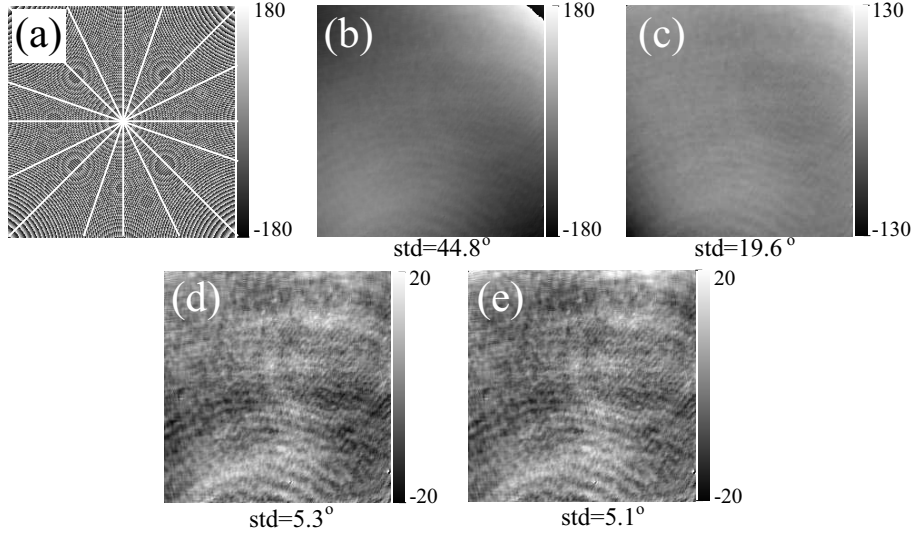


Figure 4. Phase reconstructions for increasing order of a polynomial NPL. The coefficients computed from the position of the white lines are: (a) P_{00} , (b) adding P_{10} , P_{01} , P_{20} and P_{02} ; (c) adding P_{11} ; (d) adding $P_{\alpha\beta}$ with $\alpha + \beta = 3$ and (e) adding P_{40} and P_{04} . The phase distributions reconstructed from a hologram recorded with a strongly aberrated microscope. The accuracy of the aberration compensation is measured by the computation of the phase distribution standard deviation evaluated over the entire field of view.

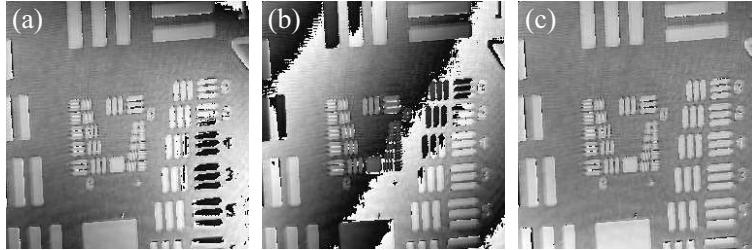


Figure 5. Phase reconstructions in perspective view of a USAF test target obtained: (a) by computing a second order NPL with the method presented in Fig. 3; (b) by using the phase reconstruction parameters (cross and non-cross-terms up to order four) calibrated using a mirror [see Fig. 4(e)] and (c) by adding a first order (tilt compensation) procedure to the phase distribution of (b).

high order and crossed terms aberrations for further uses of the microscope. Figure 5 presents the phase reconstructions, in 3D perspective views, obtained from a hologram recorded with a USAF 1950 resolution test target and with different phase reconstruction parameters. Figure 5(a) presents the reconstructed phase by computing the four parameters P_{j0} and P_{0j} ($j = 1$ to 2, second order correction) from flat areas on the specimen. As for the mirror, we see that these parameters do not compensate for the aberrations due to the introduced tilted plate. Figure 5(b) presents the reconstructed phase computed with the phase reconstruction parameters, up to order four, obtained previously with the mirror. Phase jumps appear because the tilt has changed between the two specimens. Figure 5(c) presents the result after application of a first order procedure (tilt compensation) on the phase distribution of Fig. 5(b). We can see that the aberrations are totally compensated.

7. CONCLUSION

We demonstrated in this paper that the NPL and its automatic adjustment allow the reconstruction of the absolute phase of a specimen with a single hologram acquisition. We demonstrate that this technique allows the compensation for the aberration introduced by a tilted thick plate in the setup and decreases the phase standard deviation on the entire image from 45 degrees (with the compensation of the tilt coming from the reference

wave direction and the curvature induced by the microscope objective) to 5 degrees by compensating with a higher standard polynomial order model. In this paper, we consider a standard polynomial model and a one-dimensional fitting procedure along profiles selected in known to be flat area. Future works will consider other models as Zernike polynomial model and the possibility to consider two-dimensional fitting procedure applied to entire known to be flat area. Finally, we compensate for phase aberration in the reconstruction plane, but a compensation in the hologram plane should be investigate to compensate not only for phase aberration but also to image distortion.

8. ACKNOWLEDGEMENTS

This research was funded through research grants 2153-067068.01 and 205320-103885/1 from the Swiss National Science Foundation and through research grant 6606 from the Innovation Promotion Agency (KTI/CTI).

REFERENCES

1. E. CuChe, F. Bevilacqua, and C. Depeursinge, "Digital holography for quantitative phase-contrast imaging," *Opt. Lett.* **24**(5), pp. 291–293, 1999.
2. I. Yamaguchi, J. Kato, and H. Matsuzaki, "Measurement of surface shape and deformation by phase-shifting image digital holography," *Opt. Eng.* **42**(5), pp. 1267–1271, 2003.
3. U. Schnars, "Direct phase determination in hologram interferometry with use of digitally recorded holograms," *J. Opt. Soc. Am. A* **11**, pp. 2011–2015, 1994.
4. E. CuChe, P. Marquet, and C. Depeursinge, "Simultaneous amplitude-contrast and quantitative phase-contrast microscopy by numerical reconstruction of fresnel off-axis holograms," *Appl. Opt.* **38**(34), pp. 6994–7001, 1999.
5. A. Stadelmaier and J. H. Massig, "Compensation of lens aberrations in digital holography," *Opt. Lett.* **25**(22), pp. 1630–1632, 2000.
6. S. de Nicola, A. Finizio, G. Pierattini, D. Alfieri, S. Grilli, L. Sansone, and P. Ferraro, "Recovering correct phase information in multiwavelength digital holographic microscopy by compensation for chromatic aberrations," *Opt. Lett.* **30**(20), pp. 2706–2708, 2005.
7. S. de Nicola, P. Ferraro, A. Finizio, and G. Pierattini, "Wave front reconstruction of fresnel off-axis holograms with compensation of aberrations by means of phase-shifting digital holography," *Optics and Lasers in Engineering* **37**(4), pp. 331–340, 2002.
8. S. Grilli, P. Ferraro, S. D. Nicola, A. Finizio, G. Pierattini, and R. Meucci, "Whole optical wavefields reconstruction by digital holography," *Opt. Express* **9**(6), pp. 294–302, 2001.
9. S. de Nicola, P. Ferraro, A. Finizio, and G. Pierattini, "Correct-image reconstruction in the presence of severe anamorphism by means of digital holography," *Opt. Lett.* **26**(13), pp. 974–976, 2001.
10. S. de Nicola, A. Finizio, G. Pierattini, P. Ferraro, and D. Alfieri, "Angular spectrum method with correction of anamorphism for numerical reconstruction of digital holograms on tilted planes," *Opt. Express* **13**(24), pp. 9935–9940, 2005.
11. S. de Nicola, P. Ferraro, A. Finizio, S. Grilli, and G. Pierattini, "Experimental demonstration of the longitudinal image shift in digital holography," *Opt. Eng.* **42**(6), pp. 1625–1630, 2003.
12. E. CuChe, P. Marquet, and C. Depeursinge, "Spatial filtering for zero-order and twin-image elimination in digital off-axis holography," *Appl. Opt.* **39**(23), pp. 4070–4075, 2000.
13. P. Marquet, "Dveloppement d'une nouvelle technique de microscopie optique tridimensionnelle, la microscopie holographique digitale. perspectives pour l'tude de la plasticite neuronale," 2003.
14. M. Liebling, "On fresnelets, interference fringes, and digital holography," 2004.
15. E. CuChe, P. Marquet, and C. Depeursinge, "Aperture apodization using cubic spline interpolation: application in digital holographic microscopy," *Opt. Commun.* **182**(1-3), pp. 59–69, 2000.